Chapter 2

The experimental and theoretical techniques: an introduction

## 2.1 Scanning Tunneling Microscopy and Spectroscopy

2.1.1 The working principle

The invention of the Scanning Tunneling Microscope (STM) in 1981 by G. Binning and H. Rohrer [13, 14, 15] opened a new research in surface science previously restricted to techniques operating in the reciprocal space. The working principle of an STM is based on the quantum mechanical tunneling effect. A very sharp metallic tip is approached towards a surface and kept at a distance of few Ångstroms (typically 5-10 Å) (Fig. 2.1(a)). The application of a voltage between the tip and the surface results in the flow of a small tunneling current through the vacuum barrier that decays exponentially with the tip-surface distance, z (Fig. 2.1(b),(c)). Such tunneling current is used to control the tip-sample distance (or height) z with high sensitivity. Variations of z amounting 1 Å correspond, typically, to one order of magnitude change in the tunneling current.

When the tip scans the surface along the X and Y directions, the tunneling current is measured at each point of the digital XY matrix. In the *constant current* mode, the feedback loop adjusts the distance between the tip and the surface at each point for keeping constant an initial current value (Fig. 2.1(d)). The record of the feedback signal as a function of the tip lateral position results in a map of the surface topography. An alternative scanning mode is the so-called *constant height* mode. In this case bias voltage and tip-sample distance are kept constant during the two-dimensional scan (Fig. 2.1(d)). The variations observed in the tunneling current represent the surface image. For this mode to be used it is necessary to have a flat surface, otherwise the tip might touch the steps or impurities.

2.1.2 Theory of Scanning Tunneling Microscopy

According to the Tersoff-Hamann model of an STM tunneling junction with a spherical tip [16], the current flowing between the two electrodes in first-order perturbation
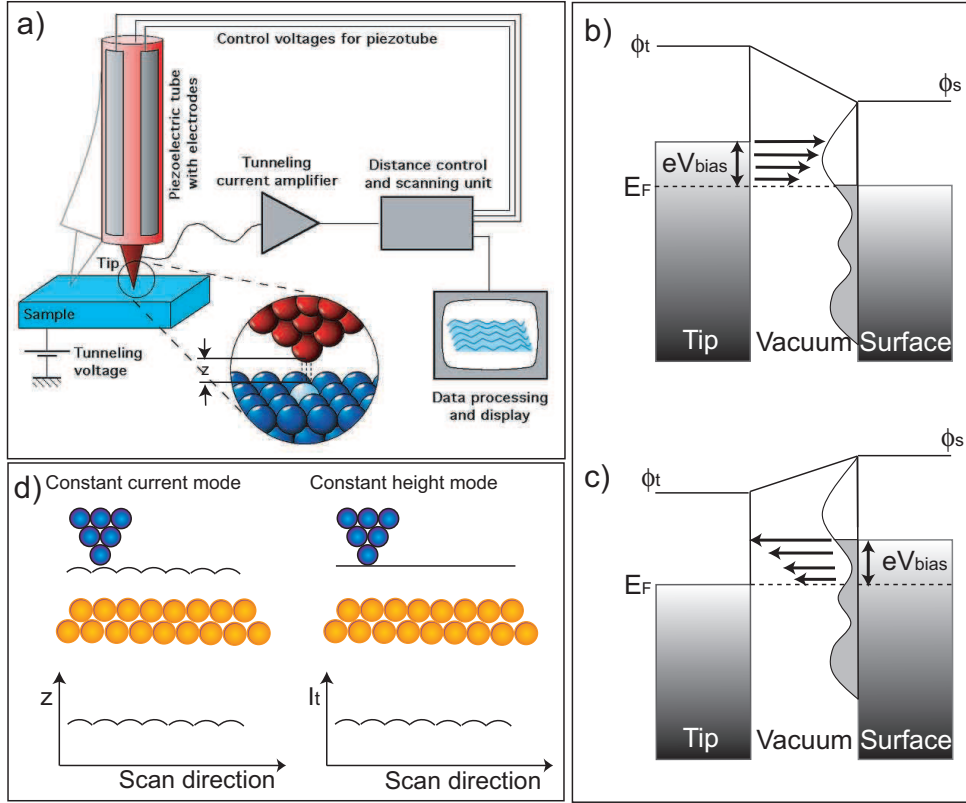
Figure 2.1: (a) Scheme of the working mechanism of an STM. Image taken from http://en.wikipedia.org/wiki/Scanning-tunneling-microscopy. The movements of the XY scanning piezos and the vertical Z height piezo are controlled by a computer. (b) Tunneling process at positive sample bias. Electrons tunnel from the tip towards the empty states of the surface in a range of energies between E_F and $E_F + eV_{bias}$. The length of the arrows indicates a proportionality to the transmission barrier coefficient at a certain energy. (c) Tunneling process at negative sample bias. The electrons tunnel in this case from the occupied states of the surface surface towards the tip. (d) Constant current and constant height scanning modes.

theory and in the limit of zero bias voltage and temperature, is given by:

$$I_t(V) = \frac{2\pi e^2 V}{\hbar} \sum_{\mu\nu} \mid M_{\mu\nu} \mid^2 \delta(E_\nu - E_F)\delta(E_\mu - E_F) \tag{2.1}$$

where $M_{\mu\nu}$, the tunneling matrix element between tip (ψ_μ) and surface (ψ_ν) states is described according to the Bardeen formalism [17], and E_F is the Fermi level. The approximation of an ideal tip with radius of curvature R, centered in r_0 and asymptotic spherical wavefunctions (s-waves) simplifies Eq. 2.1 in the following way:

$$I_t(V) \propto V \rho_t(E_F) e^{2kR} \sum_\nu \mid \Psi_\nu(r_0) \mid^2 \delta(E_\nu - E_F) \tag{2.2}$$

where $\rho_t(E_F)$ is the tip density of states, $k = \sqrt{2m\Phi_{eff}}/\hbar$ is the inverse decay length

inside a vacuum barrier with Φ_{eff} local work function, and $\sum_\nu \mid \Psi_\nu(r_0) \mid^2 \delta(E_\nu - E_F)$ is $\rho(\overrightarrow{r_0}, E)$, the surface Local Density of States (LDOS).

According to this, the tunneling current is then proportional to the Density of States (DOS) of the surface at the tip position $\overrightarrow{r_0}$:

$$I_t(V) \propto \rho(\overrightarrow{r_0}, E) \tag{2.3}$$

However, the Tersoff-Hamann formalism is extremely simplified since it is only valid for very low bias voltages and tips with spherical symmetry. A more realistic approach to the sample´s electronic structure at finite bias voltages V is obtained from a generalization of the Tersoff-Hamann tunneling current. In this case, a finite bias window between the surface and the tip is considered, and the contribution to the tunneling current by states in this energy window is integrated, including a transmission coefficient as a weighting factor [18, 19]. The tunelling current is thus expressed as:

$$I_t(V) \propto \int_{E_F}^{E_F+eV} \rho_t(E - eV)\rho_s(E)T(z, E, eV)dE \tag{2.4}$$

where ρ_t and ρ_s represent, respectively, the tip and surface density of states. The factor $T(z, E, eV)$ reveals the dependence of the transmission coefficient on the tip-sample distance, z, the energy E, and the bias voltage V. The tunneling current depends, therefore, on a combination of three factors: density of states of tip and sample and transmission coefficient. In a first approximation, reasonable for small bias, we can assume constant ρ_t and T; in this case, the tunneling current can be considered as proportional to the density of states of the surface, integrated in the $(E_F, E_F + eV)$ energy window.

2.1.3   Scanning Tunneling Spectroscopy

Following Eq. 2.4, the tunneling between tip and surface depends, for a given energy, on three interconnected parameters, i.e., the tunneling current I_t, the bias voltage V and the tip-sample distance z. Scanning Tunneling Spectroscopy (STS) measurements establishes the relations between these parameters by fixing one of them and determining the dependence between the other two. Hence, there are three modes of spectroscopy measurements: i) in I-z curves the variation of the current depending on the tip-sample distance is measured for a constant voltage V, ii) in V-z characteristics I is kept constant and the variations in z are measured for different values of V, and iii) in I-V characteristics V and I are varied while z is kept constant.

From I-z curves it is possible to obtain values of the local work function [20]. V-z curves are used to study electronic states above the vacuum barrier of the system, in the field emission regime [21]. I-V characteristics are the most widely used spectroscopic technique in the STM community. In order to take an I-V curve the feedback loop opens once the tip is positioned at a desired height. The voltage is ramped keeping a constant tip-sample distance and the tunneling current is recorded over the desired range of voltages. The changes in the slope of the obtained I-V curve reflect the conductance variations between the tip and the sample.

In this last spectroscopy technique it is usual to measure the differential conductance dI/dV with the ramped voltages. The derivation of Eq. 2.4 with respect to the bias voltage V gives the following relation:

$$
\begin{aligned}
\frac{dI}{dV} \quad \propto \quad & \rho_t(E_F)\rho_s(E_F + eV)T(E_F + eV, eV, z) + \\
+ \quad & \int_{E_F}^{E_F+eV} \rho_t(E - eV)\rho_s(E)\frac{dT(E, eV, z)}{dV}dE + \\
+ \quad & \int_{E_F}^{E_F+eV} \rho_s(E)\frac{d\rho_t(E')}{dE'}T(E, eV, z)dE
\end{aligned} \tag{2.5}
$$

If we assume both a constant tip density of states ρ_t and constant transmission coefficient in the considered energy range, the two integrals in Eq. 2.5 vanish and the expression is simplified to:

$$
\frac{dI}{dV} \propto \rho_t(E_F)\rho_s(E_F + eV)T(E_F + eV, eV, z) \tag{2.6}
$$

In general, the measurement of dI/dV is a good approximation to the LDOS of the surface at an energy value eV, being V the bias voltage applied between the surface and the tip.

The experimental detection of the dI/dV signal is done by the use of a lock-in amplifier. A small high-frequency sinusoidal signal, V_{ac}, is superimposed to the constant dc voltage. This modulation causes also a sinusoidal response in the tunneling current. The amplitude of the modulated current is sensitive to the slope of the I-V curve. Fig. 2.2 shows a scheme of how the convolution of the applied sinusoidal signal and the tunneling current can be used to detect the changes in the I-V characteristics.

For a small applied sinusiodal signal $V_{ac} = V_{mod}sin(\omega t)$, the modulated current can be expanded in a Taylor series:

$$
I(V_{bias}+V_{mod}sin(\omega t)) \sim I(V_{bias}) + \frac{dI(V_{bias})}{dV}\cdot V_{mod}sin(\omega t) + \frac{dI^2(V_{bias})}{dV^2}\cdot V_{mod}^2 sin^2(\omega t) + ... \tag{2.7}
$$

By means of a lock-in amplifier we can extract the first harmonic frequency, which is proportional to the differential conductance signal dI/dV. The detection of the second harmonic allows to probe vibrational spectroscopy d^2I/dV^2.

Another spectroscopy tool we use is the spatial mapping of the dI/dV signal in a surface area. During a slow *constant current* topography image, the dI/dV signal is simultaneously recorded in each point of the XY matrix at a certain bias voltage V. As a result, we have a mapping that reflects the LDOS of a two-dimensional region at a defined energy eV, in contrast with normal topography that involves integration of states from the Fermi level. Since the feedback loop is activated over the measurement, the frequency of the modulated signal needs to be higher than the cut-off frequency of the feedback loop response in order not to interfere with the Z-control piezo and change the tip-sample distance.
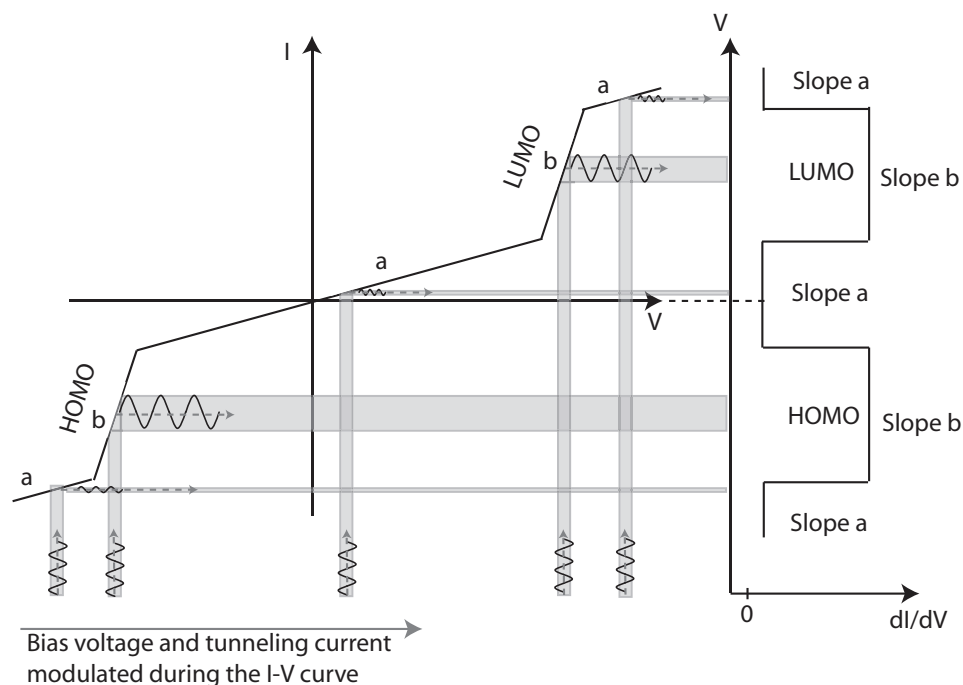
Figure 2.2: Model illustrating the operation of a lock-in. A sinusoidal signal is added to the voltage ramp, and, consequently, to the tunneling current. The modulation of the current is sensitive to the different slopes of the I-V curve. The inflexion points occurring at resonance levels (HOMO, LUMO, for example) are resolved in the lock-in as peaks, depicting the two changes of slope.

2.1.4 Tunneling processes through molecules

The adsorption of molecules on metallic surfaces introduces several complexities in the LDOS of the combined surface + molecule system that can be explored by STS. On the one hand, the molecular electronic levels are broadened into resonances and shifted due to interactions with the substrate. On the other hand, tunneling electrons may excite molecular vibrations during the tunneling process. Thus, two possible decay paths (elastic and inelastic) for electrons traveling from the tip to the surface and viceversa can be considered.

Elastic processes. In this case the electron tunnels from the tip to the surface without loss of energy. It reflects the LDOS of the molecule + surface system (Fig. 2.3(a)).

Inelastic processes. They involve phonon-mediated tunneling with electron energy loss. We can distinguish two types of inelastic processes: i) Vibronic tunneling, and ii) Inelastic tunneling. i) is a combination of inelastic and elastic processes. An electron with an energy slightly larger than an elastic channel is injected into the molecule. The electron excites vibrational modes when tunneling through the resonant molecular channel. These modes are detected as extra resonant peaks in the dI/dV signal at energies multiple of $\hbar\omega$ above the molecular resonances (Fig. 2.3(b)). In ii) electrons with energies close to the Fermi level may also

excite molecular vibrational modes. These vibrations open an extra conduction channel as presented in the scheme of Fig. 2.3(c) causing a small change in the tunneling current. The vibration excitations can be detected as symmetric steps in the dI/dV curve at energy values corresponding to the molecular vibrational modes. Normally, the steps in dI/dV are small and vibrational features are better extracted from the corresponding d^2I/dV^2 curve.
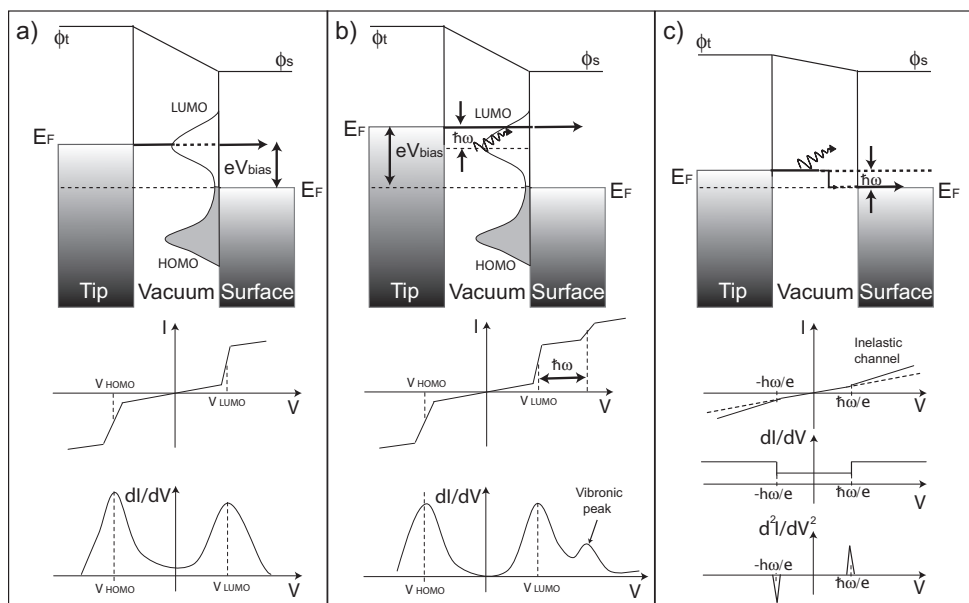
Figure 2.3: (a) Elastic tunneling. Electrons within an energy window eV_{bias} tunnel through a tip-vacuum-molecule-surface system without loss of energy. I-V characteristics present an inflexion at those points related to the molecule + surface resonances, which are resolved as peaks in the dI/dV curve. (b) Tunneling process involving vibronic excitation at a molecular orbital. The vibronic peak is resolved as a protrusion in the dI/dV spectra at energy separations of $\hbar\omega/e$. (c) Inelastic tunneling. Electrons excite a pure vibration in the molecule and lose energy. The opening of this inelastic channel increases the conductance at the value of the vibration $\pm\hbar\omega/e$. This is resolved as symmetric steps in the dI/dV curve and peaks at opposite polarities in the d^2I/dV^2 spectrum [12].

2.2   Brief introduction to Density Functional Theory

Some of the experimental results presented along this thesis have an important theoretical support by means of Density Functional Theory (DFT) calculations. This section is devoted to briefly introduce the basic concepts we have used throughout the present work.

DFT calculations are based in the energy minimization using approximate functionals of electron density that provide a useful balance between accuracy and computational cost. In DFT this functional is related to the electronic density of a system of interacting particles [22]. The pillars of the theory are:

The Hohenberg-Kohn theorems. They establish that there is a one-to-one mapping between the ground state electronic density and the ground state wave function [23]. Therefore, the calculation of the density can be replaced by a calculation of the wave function which defines the system. The introduction of the density as the main variable is an important simplification compared to, for example, Hartree-Fock (HF) calculations of a system formed by N particles: while the degrees of freedom of the HF wavefunctions are 3N, the density of DFT only depends on three spatial variables for the static case.

The Kohn-Sahm equations. They consist on a set of self-consistent one-electron equations based on the Hohenberg-Kohn theorems. They have the same electron densities as the physical system and replace the unsolvable many-electron problem [24]. In these equations, the interaction among electrons is simulated via an effective potential due to the surrounding electrons.

Exchange-correlation functionals. Since no exact functionals for exchange and correlation are known (except for the free electron gas) some approximations have to be included in order to calculate physical quantities. Basically, two approximations are used in DFT: (i) Local-density approximation (LDA), that assumes that exchange-correlation is local [25], and (ii) Generalized gradient approximation (GGA), that takes density variations into account .

DFT calculations provide good estimations for several physical properties of a metal-organic interface, like atomic structure, workfunction, vibrational modes, chemisorption energies, and charge transfer between molecule and surface. By projecting the DOS onto states of the different parts of a system (for example, molecular orbitals or surface states) their relative weight in the electronic structure of the complete system can be extracted [26]. The mathematical expression that defines the projection of the DOS $\psi_\alpha(r)$ on an orbital $\psi_a(r)$ is:

$$\rho_a(\varepsilon) = \sum_\alpha |<\psi_\alpha|\psi_a>|^2 \delta(\varepsilon - \varepsilon_\alpha) \tag{2.8}$$

In our systems the total DOS corresponds to the combination of surface and molecules. By projecting the total DOS on the molecular orbitals of the free molecule we obtain information about orbital alignment with respect to E_F (charge transfer) and broadening (hybridization) of orbitals due to surface-molecule interactions (Fig. 2.4).

A second tool that will be used in the analysis of our results is the induced electronic density. DFT can calculate the total electronic density of the complete system and also of the individual constituents with the atomic configuration they have in the full relaxed system. By substracting the individual contributions from the total density we obtain the density of charge which is induced in each part of the system when they interact, thus allowing to trace the charge displacements occurring upon their interaction.
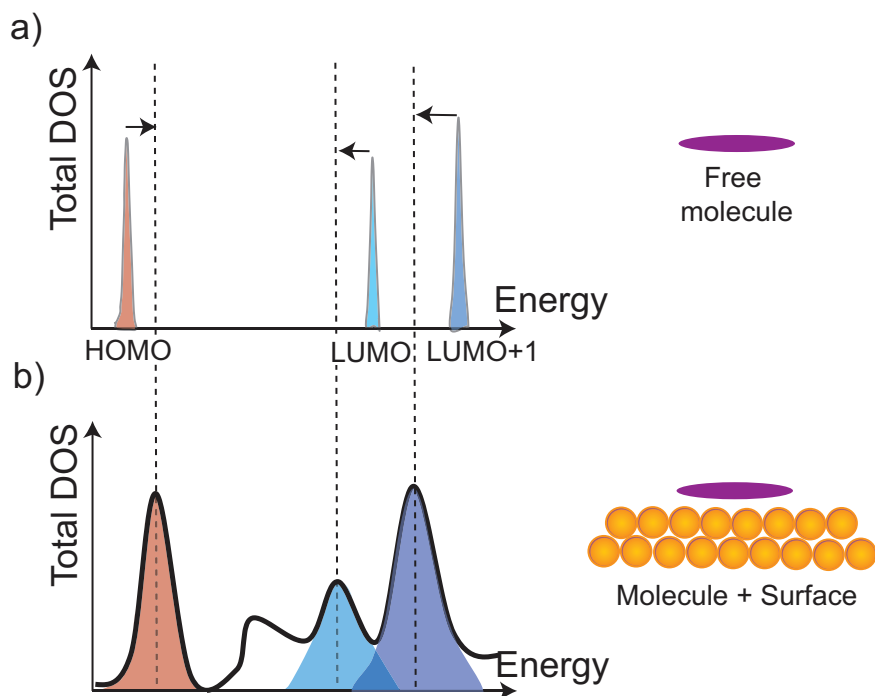
Figure 2.4: Illustrative scheme of the working principle of PDOS. Molecular orbitals of free molecules consist on thin, δ-Dirac like resonances (upper figure). When deposited on a surface, the molecular levels shift by charge transfer processes, and broaden due to interactions with the substrate. The projection of the total DOS of the whole molecule + surface system onto the free molecule orbitals (color shadows) allows to trace the nature of the broad features.

2.3   The Au(111) surface

The surface used throughout this thesis is Au(111). This close packed surface exhibits the so-called herringbone reconstruction created by the inclusion of an "extra" atom every 22 atoms along the $[1\bar{1}0]$ direction. As a consequence of this, the surface layer is stressed and presents a corrugation along that surface direction. The $(22 \times \sqrt{3})$ unit cell alternate regions with atoms on bulk-like (fcc) sites and atoms on (hcp) sites. Such areas are separated by stacking faults and partial dislocations of the compressed topmost layer called soliton-lines (Fig. 2.5(a)). The surface is therefore non-planar, having a corrugation of 0.2 Å. The direction of these lines along the $[11\bar{2}]$ direction rotates periodically by 120° and creates the characteristic zig-zag structures (Fig. 2.5(b)) that in many cases pattern the organization of physisorbed adsorbates on the surface, as demonstrated by adsorption commensurabilities with the herringbone structure [27]. The elbows of the herringbone reconstruction are areas of lower potential, therefore preferential adsorption sites for adsorbates [28, 29].

The reconstructed Au(111) surface presents a two-dimensional Shockley surface-state band [30], with binding energy 490 meV below the Fermi level [31]. The long periodicity imposed by the herringbone superlattice creates a spatial and energetic
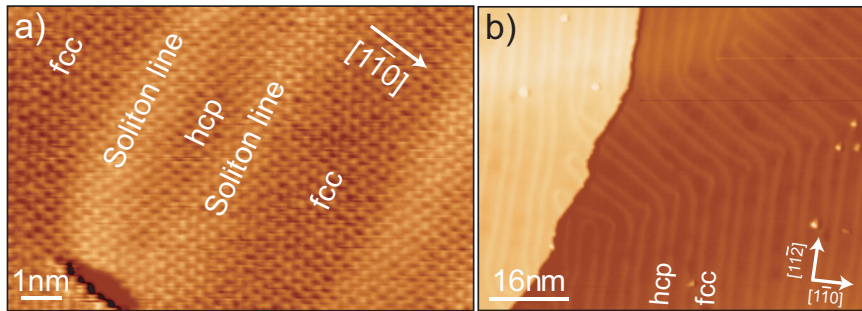
Figure 2.5: (a) Atomically resolved STM image revealing the atomic arrangement along the [1$\bar{1}$0] direction that divides the surface in different regions separated by higher soliton lines (V = 1.2 V, I = 14 nA). (b) Large STM image showing the Au(111) herringbone reconstruction on the surface (V = 0.86 V, I = 0.9 nA).

rearrangement of the surface-state causing a binding energy difference amounting to $\sim$ 25 meV between fcc and hcp regions of the reconstruction [32].

2.4 Imaging molecules with STM

Since the first observations of organic molecules adsorbed on surfaces [33, 34, 35], STM has been widely used to characterize the physical and chemical mechanisms involved in both the molecular adsorption and the structure of molecular thin films on surfaces. However, the interpretation of molecule + surface STM images is not straightforward. First of all, STM images are not a pure topography map but include also electronic information of both the molecule and the underlying surface. One good example is the case of carbon monoxide (CO) adsorbed on a metallic surface [36, 37]. With a metallic tip the molecule is imaged as a depression. This result does not correspond with a naif topography interpretation of the STM imaging capability and more complex explanations have to be taken into account. For the specific case of CO molecules, the imaging entails a depletion of the metallic states due to the molecule-metal bonding [38]. Hence, especially for the case of chemisorbed systems, STM images carry information about the chemical molecule-surface bonding, that only throughout detailed theoretical simulations can be extracted.

Molecules are characterized by a HOMO-LUMO gap [1], which in some cases is several eV wide. By scanning at energies close to the Fermi level these molecules should appear "transparent" to the tip since no tunneling of electrons would occur inside the gap. However, the interaction with the surface broadens the molecular levels as shown in Fig. 2.4 and results in the formation of extended tails that contribute to the LDOS at energies close to E_F. In consequence, molecules can be imaged, normally as featureless protrusions, in the STM junction at low energy values. When the eV_{bias} applied between tip and surface reaches the energy of a molecular resonance the topography image may show intramolecular resolution. In some cases, usually for weakly adsorbed molecules, the resonant tunneling through the HOMO/LUMO derived resonances be-

---

[1]HOMO: Highest Occupied Molecular Orbital, LUMO: Lowest Unoccupied Molecular Orbital.

comes the predominant contribution to the current. The topography image resembles in these cases the spatial shape of the free-molecule orbitals, as obtained by theoretical simulations (Fig. 2.6).
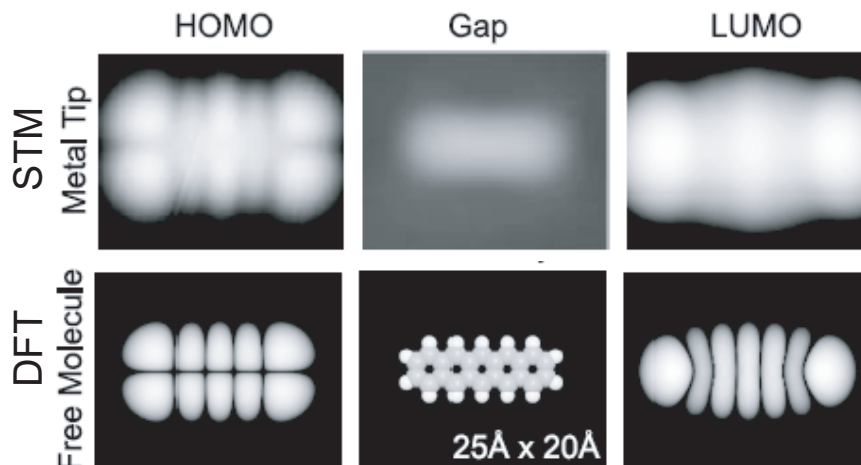

Figure 2.6: [39] Comparison between experimental and theoretical imaging of a pentacene molecule adsorbed on an ultra-thin insulating NaCl layer. STM imaging in the HOMO-LUMO gap results in the obtention of featureless protrusions, whereas the imaging at voltages exceeding the HOMO (left) and LUMO (right) exhibit very pronounced features, corresponding to the DFT calculations at the correspondent energies.

In most of the cases organic molecules are imaged as protrusions in the STM topography maps, but the height observed seldom corresponds to the physical height of the molecule. The "apparent height" of a molecule exhibits variations for different tunneling voltages, increasing drastically when a resonant channel is available, for example, at the HOMO/LUMO levels. Variations are also expected for molecular imaging on different surfaces, like from metal to thin-film insulators, due to different locations of the molecular orbitals and distinct extensions of the tails of molecular resonances.

2.5 Experimental set-up and details

The STM and STS measurements here presented were taken in a Low-Temperature STM designed by Dr. Gerhard Meyer and Dr. Sven Zöphel [40] and built by Christian Roth and Dr. Micol Alemani [41]. The experimental system consists on two ultra-high vacuum (UHV) chambers (Fig. 2.7(a),(b)). The preparation chamber is equipped with the standard UHV preparation tools: mass spectrometer, sputter ion-gun, and a home-made Knudsen cell evaporator (attached to the load lock). The STM chamber contains the STM scanner. It is of Besocke "beetle" type and it works in contact with a liquid-He bath at an equilibrium temperature of 4.8 K. It is isolated from mechanical vibrations via stainless steel springs, eddy current damped. Further damping against low frequency vibrations is achieved by pneumatic feet that lift the whole chamber during the data acquisition. STS measurements are recorded with an external com-

mercial Stanford Research SR830 lock-in amplifier. The STM data are analyzed with the WSxM software [42].
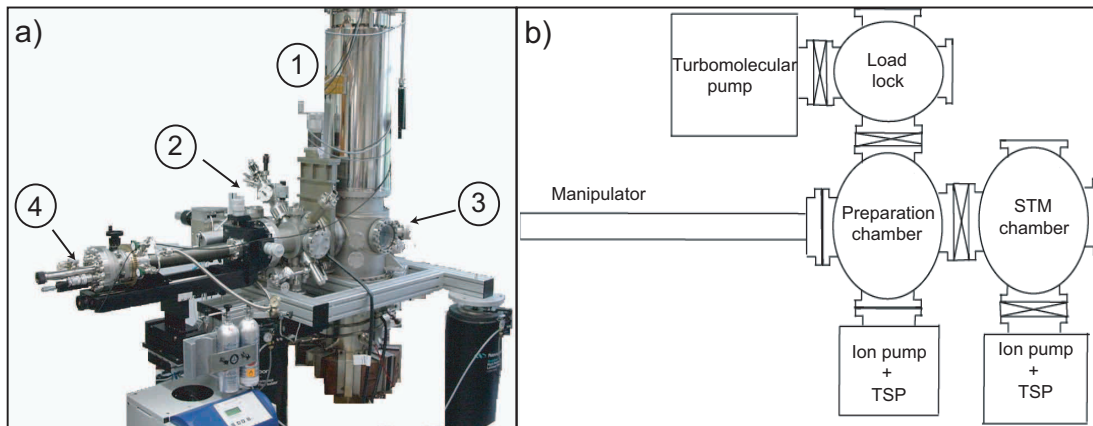
Figure 2.7: Photo (a) and scheme (b) of the UHV system. (1) is the liquid He cryostat, (2) the preparation chamber, (3) the STM chamber and (4) the manipulator that connects (2) and (3).

The growth of the heteromolecular structures is done on an atomically clean Au(111) surface by molecular sublimation from a home-made Knudsen cell.

The Au(111) sample is cleaned under UHV conditions by multiple sputtering-annealing cycles. The sample is sputtered with Ne ions with 1.5 keV energy at room temperature for, typically, 30 minutes. Subsequently, it is annealed at a temperature of ~ 750 K for a period of 15 minutes. This process is repeated several times until the surface is free from impurities.

All the molecules used in these thesis, C_{60}, TPC, TTF and TCNQ, are commercially available at Aldrich. They are sublimated from a home-made evaporator that consists on three crucibles with independent heating. In order to avoid thermal cross-talking, the crucibles are located into a water-cooled copper block. The sublimation of each compound can be performed either in a sequential fashion (method followed in the preparation of all the systems presented in this thesis) or simultaneously. The sublimation temperatures in UHV conditions are shown in Fig. 2.8 for each molecule [2]. Previous to sublimation, each molecular compound is outgassed by a short annealing (10-20 minutes) at typically 10-20°C above the temperature used for sublimation.

In the case of the TTF and TCNQ ultra thin-film preparation we used either independent TTF and TCNQ powders or the TTF-TCNQ molecular compound. The sublimation temperatures in UHV conditions for individual TTF and TCNQ are, respectively, room temperature and 120°C. In the case of the mixed TTF-TCNQ these temperatures are slightly different: TTF sublimates around 70°C and TCNQ at 140°C (Fig. 2.8). Therefore, the individual growth at low coverage of TTF can be performed in a better controlled manner by using the mixed TTF-TCNQ transfer salt, at temperatures below the sublimation of TCNQ (140°C). For temperatures higher than 140°C,

---
[2]At these temperatures the molecular coverage on the Au(111) surface is, typically, 0.1 monolayers (ML) after ~ 1 minute of exposure

co-sublimation of both TTF and TCNQ is obtained from the mixed compound but it is accompanied by a higher deposition rate of TTF than TCNQ. The preparation of TTF-TCNQ thin films is thus mainly done by previously depositing TTF from the mixed compound and followed by a subsequent addition of TCNQ from pure powder.

Molecule		Sublimation Temperature (°C)
TPC		75-85
Fullerene		420-450
TTF (Pure)		Room temperature
TCNQ (Pure)		120
Mixed TTF-TCNQ Compound	TTF	70-80
	TCNQ	140

Figure 2.8: Sublimation temperatures used for the deposition in UHV conditions of the investigated molecules. TTF and TCNQ have different vapor pressures for the pure powder and the mixed compound.

In this thesis we work with molecular systems whose components present different diffusion barriers. In general, for sufficiently low substrate temperatures, molecular diffusion is hindered and the adsorbates are pinned at their initial adsorption places. When the temperature is increased, diffusion is allowed and molecules can find their most stable adsorption places. Therefore, the control of the surface temperature during deposition is important in the formation of distinct self-assembled systems. The substrate is attached to a commercial Vab manipulator during both surface cleaning and molecular deposition processes [41]. The head of the manipulator includes a cryostat especially designed for being cooled through a flux of liquid He. The surface can be cooled to a minimum temperature of 70 K. The control of the He flux allows molecular deposition in a temperature range between 70 K and 300 K. Once the molecular system is deposited at the desired surface temperature, the sample is cooled down to 70 K and is inserted in the STM chamber.